Metal Deportment in Complex Secondary Raw Materials: The Case of Vanadium in Basic Oxygen Furnace Slags

A. D. Renno[1] · R. Möckel[1] · M. Frenzel[1] · D. Ebert[1] · K. Bachmann[1] · J. Krause[1] · J. Gutzmer[1]

Abstract

With the increasing demand for metalliferous and mineral raw materials and the consequent depletion of the global natural resource base, the possible utilization of secondary raw material sources is receiving more and more attention. In the present study, we present results from a detailed vanadium deportment study of three basic oxygen furnace slag (BOS) samples known to containing elevated bulk concentrations of vanadium. Complementary analytical methods that were used to quantify the abundance and composition of V-containing phases include SEM-based automated mineralogy, X-ray fluorescence analysis, and X-ray powder diffraction as well as electron probe microanalysis. The vanadium deportment was quantified using Monte-Carlo simulations of the data obtained from automated mineralogy and electron microprobe analysis. The total V concentrations identified by XRF are between 1.7 and 2.2 wt.% V. The most important hosts of vanadium are larnite-, brownmillerite- and portlandite-solid solutions. In two samples Ca carbonates also significantly contribute to the V deportment, while wuestite, lime, and native iron do not contribute significantly to the vanadium deportment. A thorough consistency check identifies considerable uncertainties in the density of the V-bearing phases as the most likely reason to explain remaining discrepancies between measured and calculated V values.

Keywords Steel slag · Basic oxygen furnace slag · Vanadium-bearing slag · Vanadium · Vanadium deportment

1 Introduction

Associated with global steel production approaching 2 billion tons per annum (2022: 1885 million tons [1]), there is a similar increase in the amount of steel slags generated (2017: 500 million tons [2]). In an effort to increase sustainability of steel production, this slag needs to be either recycled or even up-cycled. Although steel slags are generally classified as non-toxic [3, 4], they do constitute both an economic and environmental problem. The degree of utilization of steel slags varies greatly; although it reaches 80% in some countries, its utilization is usually much lower with the remainder landfilled [2, 5]. The most common use of steel slags is as construction material. This application is, however, limited in some cases by elevated concentrations of metals such as chromium (Cr) and vanadium (V) [6]. This is because these two metals occur in different oxidation states resulting in a significant ecotoxicological risk. This risk pertains in particular to the uncontrolled release of Cr^{VI} and V^{V} from steel slags into natural systems through weathering processes [7–11]. Because vanadium and chromium are also both considered critical raw materials [12, 13], there have recently been intensive efforts to develop approaches to recover both vanadium and chromium from steel slags [7, 14–16]. It is the goal of this research to not only recycle V and Cr but also to make the remaining slag material amenable for further utilization.

There are several technological approaches to recover vanadium (and other valuable elements) from BOS. Current overviews can be found in [14] and [15]. Despite the fact that the phase composition of V-bearing BOS is well studied [17], there is a lack of knowledge concerning the deportment, e.g., the distribution of vanadium between the different phases present in the slag. The value of such deportment studies has been well documented for primary raw materials [18–21] (and references therein). This contribution takes a similar approach to [18] in order to quantify the distribution of vanadium in several examples of vanadium-rich basic

✉ A. D. Renno
a.renno@hzdr.de

1   Helmholtz-Zentrum Dresden-Rossendorf, Helmholtz-Institute Freiberg for Resource Technology, Chemnitzer Str. 40, 09599 Freiberg, Germany

oxygen furnace slag (BOS). Such quantitative knowledge of phase composition and phase chemistry (and the variability of these compositional attributes) provides the key to develop innovative approaches for the efficient extraction of vanadium from BOS. This study also provides a comprehensive workflow to assess metal deportment in complex secondary raw materials such as hygroscopic steel slags.

1.1 Steelmaking and Steel Slags

Most steel is produced via two basic processes: the so-called "primary" blast furnace-oxygen-base furnace (BF-BOF) route and the "secondary" electric arc furnace (EAF) route. Blast furnaces (BF) produce iron from iron ore by reduction with coke. In a second step, the iron is then processed into steel in an oxygen converter. In the latter process, hot metal, steel scrap, and flux are charged into the converter furnace. Pure oxygen is added via a water-cooled lance to this furnace charge. The oxygen reacts with the silicon and carbon dissolved in the hot metal. CO_2 is generated and escapes as a gas phase while SiO_2 forms a liquid slag phase that is then separated from the steel.

Electric arc furnaces produce steel mainly from scrap with possible minor amounts of solidified iron or sponge iron. The heat required to melt the metal is generated by an arc produced by graphite electrodes in contact with the metal. Arc temperatures reach up to 3500 °C, while the temperature of the molten metal is around 1800 °C.

Due to these technological differences, steel slags are mainly divided into "oxygen steelmaking slags" and "electric arc furnace slags" or synonymously "basic oxygen furnace" (BOS) and "electric furnace" (EF) slags [22, 23].

Basic oxygen furnace slag (BOS) (also called LD-converter slag) forms during the production of steel in a basic oxygen furnace by blowing oxygen into the metal from the blast furnace to remove carbon and other elements that have a high affinity to oxygen. The slag formation needs the addition of fluxes such as lime (CaO) or calcite ($CaCO_3$) and/or dolomite ($CaMg(CO_3)_2$) that lead to the formation of liquid slag by reaction with silicates and oxides of the furnace feed. Figure 1 shows the reaction path in the system FeO-CaO-SiO_2-Al_2O_3-MgO [22] during the addition of the Ca-rich flux.

When the reaction process is complete, the molten crude steel accumulates at the bottom of the furnace and the liquid slag rises to the top. The crude steel and slag are then tapped into separate ladles/pots at temperatures > 1600 °C. The slag is in this way separated from the crude steel.

The composition of BOS in terms of its major components is well represented by the system FeO-CaO-SiO_2-Al_2O_3-MgO [2, 24]. The chemical composition of typical BOS (Table 1 and Table A 1) is extremely variable but always dominated by high CaO contents [25, 26].
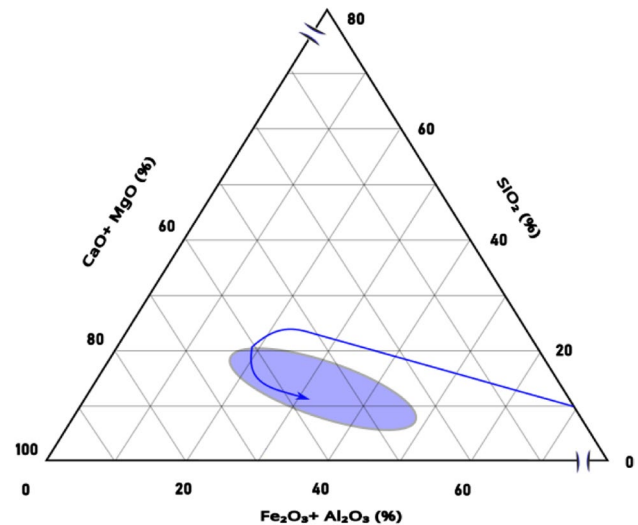
Fig. 1 Generalized reaction path of the formation of BOS in the system $SiO_2 - Fe_2O_3 + Al_2O_3 - CaO + MgO$ during the adding of the Ca-rich flux (blue arrow) as well as the range of compositions (blue area) of BOS. Adapted and simplified from [2, 22, 24, 25]

Table 1 Range of the chemical composition of BOS reported in literature [26]

Sample	Summary [26]			
wt.%	Min	Max	Average	SD
Al_2O_3	0.02	20.56	3.6	4.6
CaO	19.0	60.4	44.2	8.5
FeO_{total}	10.0	35.0	24.6	6.2
K_2O	0.027	1.23	0.2	0.4
MgO	0.82	28.0	7.5	5.1
MnO	0.28	8.48	3.9	1.8
Na_2O	0.036	0.25	0.1	0.1
SiO_2	0.23	24.41	12.0	4.2
TiO_2	0.3	2.0	0.8	0.4
S	0.02	0.5	0.1	0.1
P_2O_5	0.11	4.58	1.8	1.15
LOI	0.3	7.54	2.5	2.7
$mg*kg^{-1}$				
Cr	240	23,000	3172	5954
Ni	2.1	25	10.5	10.2
V	68	25,100	5094	8292
Zn	8.5	200	105	82.9

Depending on the composition of the primary or secondary raw materials used in steel production, some of the slags may contain significant amounts of minor elements such as P, V, Cr, Zn, Ni, and Ti. Some of these can occur in multiple oxidation states in BOS [27, 28]. For the current

Table 2 Mineralogical composition of different types of BOS reported in literature [30–32]

Name	Chemical formula	BOF various [30]	BOF [31]	BOF "fresh" [32]
Larnite	$\beta\text{-}Ca_2SiO_4$	38.1–52	30.8	21.5–22
$\gamma\text{-}Ca_2SiO_4$	$\gamma\text{-}Ca_2SiO_4$			7.3–7.9
Srebrodolskite	$Ca_2Fe_2O_5$		32.3	31–37.2
Ca-ferrite	$CaFe_2O_4$	20.2–30.3		
Wuestite	FeO	11.5–13.1	6.7	1.1–2.2
Portlandite	$Ca(OH)_2$	1.1–7.3	3.1	
Lime	CaO	2–8.1	8.8	10.6–20.6
Iron	Fe			0.3–0.4
Enstatite	$Mg_2Si_2O_6$		1.9	1.9–3.8
Hematite	Fe_2O_3			2.0–4.1
Magnetite	Fe_3O_4			0.4–0.8
(Mg)-ferrosilite	$FeSiO_3$		2.2	2.8–3.6
Fayalite	Fe_2SiO_4		3.8	4.2–5.5
Wollastonite	$CaSiO_3$		2.9	0.7–1.1
Periclase	MgO		1.1	0.7–1.6
Calcite	$CaCO_3$	1.9–4		
Quartz	SiO_2	0–10.9		1.4–2.8
"Other"		6.4		

study, it is important to note that vanadium can occur in two oxidation states (V_2O_3 and VO_2) in BOS [29].

Vanadium-rich slags result from the smelting of vanadium-bearing magnetite (Fe_3O_4) in BFs [14]. Another possible source of vanadium in these slags is vanadium-rich so-called HSLA (high strength-low alloy) steel scrap. However, since steel scrap is only added to a small extent to the basic oxygen furnace charge, it is safe to assume that vanadium-bearing magnetite is the main source of vanadium in BOS.

The phase composition of BOS is mostly determined by its CaO content, the CaO/SiO_2 ratio, and cooling kinetics. Typical phases occurring in BOS [30–32] are listed in Table 2.

2 Materials and Methods

2.1 Samples

Three bulk slag samples were provided for study by a potential user of BOS from two different sites, designated here by the codes O and R (Table 3). Figure 2 shows an example of the appearance of the investigated samples. Details on sampling are not known, but according to information from the supplier and owner of the slag dumps, the samples were taken in such a way that they can be considered as representative of three sampled dumps. All samples had a small to moderate moisture content because the samples had already been exposed to surface weathering for a longer period of

Table 3 BOS samples included in this study

Sample	Origin	Weight [kg]
O-1	Slag heap "O"	1048
O-2	Slag heap "O"	1050
R-1	Slag heap "R"	1166
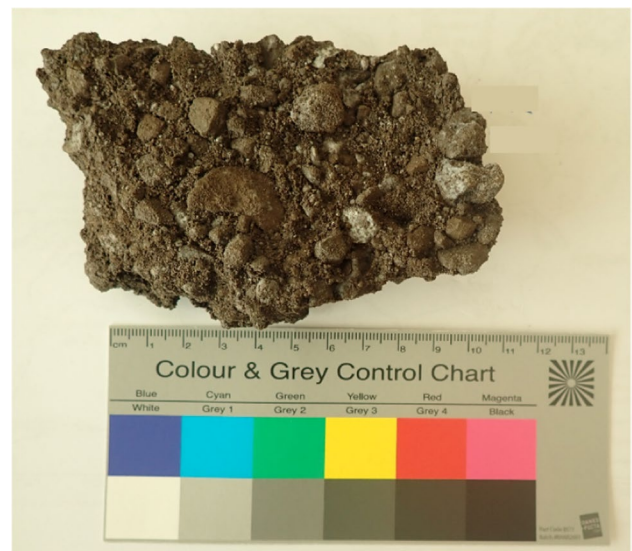
Fig. 2 Slag sample O-1 before crushing and homogenization. Note vastly different particle sizes from sub-millimeter to centimeter range. White efflorescence formed on the surface of coarse particles in response to drying in the laboratory prior to grinding

time. Fresh, not stockpiled material, was not included in the investigations, since the weathering effects were to be taken into account in the deportment analysis.

2.2 Sample Preparation

Comminution of the bulk slag samples was performed in a multistage process. Slag particle sized ranged from sub-millimeter to centimeter range (Fig. 2) and required grinding prior to further treatment. Samples O-1 and O-2 were crushed to a d(80) value of 1 mm and sample R-1 to a d(80) value of 1.4 mm by means of a combination of jaw crusher, hammer crusher, and roller crusher. Sample R-1 showed strong agglomeration after each comminution step, which led to "clogging" of the sieve trays and other mechanical parts. However, extensive drying of the sample material could likely have prevented such agglomeration. Drying at elevated temperature was, nevertheless, avoided in order to preserve the primary phase composition. The sensitivity of the BOS to changes in humidity is aptly illustrated by the formation of white efflorescent crusts during drying under ambient conditions in the laboratory (Fig. 2).

Following the initial comminution step, homogenization and separation of representative sample fractions for further sample preparation and analysis were carried out using rotary splitters of different sizes and with different sample throughput. Finally, five representative sub-samples of about 1 kg each were available for every one of the three BOS samples. The sub-samples were further split using smaller rotary sample splitters to yield sample amounts necessary for different analytical methods. Further sample preparation steps are reported below—together with the respective analytical methods used.

2.3 X-Ray Fluorescence Spectrometry (XRF)

Wavelength dispersive XRF (WD-XRF) was used to determine the bulk chemistry of the three BOS samples. For the preparation of glass beads, around 3 g of sample material was first used for the determination of the loss on ignition (LOI). LOI was determined in a muffle furnace at 950 °C for 2 h. Since the samples remained hygroscopic after delivery and during all sample preparation steps, the LOI values determined can only be considered as "snapshots." In order to estimate the maximum water absorption of the investigated BOS, one representative sample from each sample set was exposed to a water-saturated atmosphere for several weeks and the LOI values were determined again. One gram of this precalcined material was then thoroughly mixed with 8 g of LiB_4O_7 as fusing flux and melted in an automatic CLAISSE TheOx oven in platinum crucibles. This melt was then used to cast glass beads for XRF analysis.

WD-XRF analysis was carried out using a PANalytical Axios mineral spectrometer, equipped with a Rh-tube. The respective parameters are adjusted between 25–60 kV and 66–160 mA, depending on the element. The data were obtained from the fully calibrated WROXI program, provided by the manufacturer. All elements were in the designated calibration range. The elements analyzed, including the limits of determination, are summarized in Table A 2.

2.4 X-Ray Powder Diffraction (XRD)

Aliquots of around 3 g of the material were used for XRD analysis. The material was wet-milled with ethanol using a McCrone micronizing mill. The powders were then filled into sample holders by the so-called back-fill method [33].

X-ray powder diffraction measurements were done using a PANalytical Empyrean diffractometer, equipped with a Co-tube and a PIXcel 3D medipix 1 × 1 area detector. The tube was operated at 35 kV and 35 mA. An iron filter on the primary beam side was used to suppress K-beta radiation. The irradiated area on the sample was kept constant at 12 × 15 mm² by means of an automated divergence slit. The measured 2-theta range was set 5 to 80° at a step size of 0.0131° 2-theta. Overall measurement time was about 2 h 30 min per sample. Phase identification was done using the ICDD PDF-4 + database, while quantification was performed via the Rietveld method using the Profex/BGMN v. 4.1 [34] software bundle.

2.5 SEM-Based Automated Mineralogy (AM)

For quantitative mineralogical analysis using SEM-based automated mineralogy (AM) and electron probe microanalysis (EPMA), a total of 15 polished grain mounts with a diameter of 30 mm were prepared. The process involved mixing the sample material with graphite powder and epoxy resin. The resulting mixture was used to create epoxy blocks, which were then cut into five slices. Each slice was rotated 90°, reembedded in epoxy resin, and polished following the established protocol outlined in [35]. Figure 3 shows a typical grain mount of the sample series. The resulting grain-mount sample numbers used in the EPMA and AM analyses are summarized in Table A 3.

Following carbon coating of the polished sample surface, AM measurements were conducted using a Mineral Liberation Analyzer (MLA) [36] instrument. The MLA instrument utilized in this study consisted of a FEI Quanta 650F field emission scanning electron microscope equipped with two Bruker Quantax X-flash 5030 energy-dispersive X-ray detectors, along with the MLA software suite (version 3.15). The GXMAP measurement mode [37, 38] was implemented, employing an acceleration voltage of 25 kV, an image resolution of 1 μm/pixel, a step size of 6 pixels,
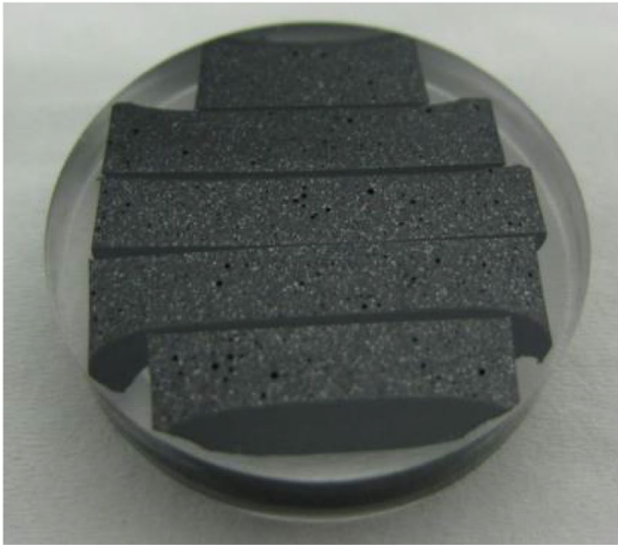
Fig. 3 Polished sample block for AM and EPMA analysis (diameter 2.5 cm) before carbon coating (example) (© Dirk Sandmann)

and backscattered electron beam (BSE) brightness calibrated on Cu. AM analyses were carried out on 15 epoxy blocks (5 blocks of each O-1, O-2, and R-1, respectively), aiming for a sufficient amount of particles to improve particle statistics for the subsequent deportment calculation.

Phases were identified based on their EDX spectra. Phase identification was carried out until the total content of unknown phases was lower than 0.25 wt.% in all samples after processing. Phase identification and sample characterization were particularly challenging due to the compositional heterogeneity of the slag samples and strong zonation of certain phases. Hence, electron probe microanalysis (see below) was used to refine the mineral standard list used for phase classification. For more details of this procedure, see [38]. The list of mineral standards (see Table A 17) is different from the list of phases that was ultimately used for the deportment analysis. The latter combines different phases—mostly those that represent different members of a continuous solid solution series (see Table 6).

2.6 Electron Probe Microanalysis (EPMA)

The chemical composition of phases from two representative grain mounts of each sample was determined with a JEOL JXA 8530F electron probe microanalyzer equipped with a field emission electron gun and five wavelength dispersive spectrometers. Operating conditions were set at 20 kV and 25 nA, with a beam diameter of 1 to 10 μm, respectively. Matrix corrections were done using the ZAF method. An additional correction was made for peak overlaps following the procedure described in [39]. Corrections were made for the following overlaps: V-Kα by Ti-Kβ, Cr-Kα by V-Kβ, Cl-Kα by Mo-Lγ, S-Kα by Mo-Lα, S-Kα by Co-Kα 3rd

order, Mo-Lα by S-Kα, and P-Kα by Mo-LL. Further analytical details regarding the reference materials used for calibration, measured X-ray lines, dwell times on peak, and background positions can be found in Table A 4. Major elements with concentrations above 5 wt.% were corrected for machine drift assuming linear drift between two successive analyses of reference materials measured as unknowns (periclase, diopside, magnetite, rhodonite, vanadium metal, and plagioclase from ASTIMEX Ltd.). Concentrations below the quantification limit calculated by the JEOL software were excluded from the dataset, as well as concentrations with relative 2SD above 20% and obvious mixed analyses.

3 Results

3.1 Chemical Composition

The chemical composition of the samples in terms of their major components is summarized in Table 4. A complete summary of all analytical values is provided in Table A5. The comparison of the LOI values "as delivered" and "hydrated" is shown in Table A6. These results show that the maximum water contents can reach three to four times the LOI values reported for the samples in Table 4. This fact must be taken into account when evaluating the deportment data.

To ensure comparability of the results and a uniform basis for the deportment analysis, the chemical composition is presented in recalculated "anhydrous form" and then normalized to 100 wt.%.

The chemical compositions of the three slag samples are within the range of typical BOS (see Table 1 and A 1 for comparison). Vanadium contents range between 1.7 and 2.2 wt.% in all three samples—well above the average reported for BOS. In addition, the three slag samples are rather poor in P_2O_5 and sulfur, while chromium contents are close to the global average for BOS.

Comparison of the three samples illustrates the two samples O-1 and O-2 to be of rather similar chemical composition. The R sample, on the other hand, is marked by distinctly lower concentrations of MgO and Cr_2O_3, but higher contents of CaO, V, alkali elements, and phosphorus. The significant difference in CaO and MgO contents is reflected in the Ca/Mg ratio that has a value of 28 in the R sample, but only around 5 in the two O samples. Despite the overall low sample number of 5 sub-samples per sample, a significance test (one-way ANOVA) was performed to estimate whether the measured differences between the different BOS were significant. The results are presented in Table A 7 and show that almost all differences are statistically significant at the 0.05 level. This illustrates that the results of the analytical

Table 4 Chemical composition of the BOS in terms of the key components determined by WD-XRF. The reported results have been recalculated as "water-free" and normalized to 100%. Therefore, LOI is listed for information only. The limits of determination of the method are listed in Table A2

Sample	LOI	SiO_2	TiO_2	Al_2O_3	Fe_2O_3	Mn_3O_4	MgO	CaO	Na_2O	K_2O	P_2O_5	SO_3	V[§]	Cr_2O_3
O-1–1	3.5	11.13	1.29	1.56	26.79	3.60	9.84	41.63	0.01	0.02	0.46	0.25	**1.67**	0.42
O-1–2	3.6	11.29	1.30	1.57	25.56	3.68	10.08	42.31	0.01	0.02	0.47	0.25	**1.69**	0.43
O-1–3	3.8	11.36	1.31	1.56	25.21	3.68	10.08	42.57	0.01	0.02	0.47	0.25	**1.70**	0.42
O-1–4	3.9	11.34	1.33	1.60	25.31	3.68	10.03	42.48	0.01	0.02	0.47	0.25	**1.70**	0.42
O-1–5	3.8	11.30	1.31	1.59	25.66	3.65	10.00	42.29	0.01	0.02	0.47	0.25	**1.68**	0.43
O-2–1	2.2	10.89	1.18	1.30	25.62	3.29	8.90	44.27	<0.01	0.02	0.46	0.15	**1.78**	0.71
O-2–2	1.9	10.97	1.19	1.33	24.94	3.32	9.03	44.63	<0.01	0.02	0.46	0.16	**1.79**	0.72
O-2–3	2.0	10.95	1.20	1.31	25.02	3.35	9.02	44.59	<0.01	0.02	0.46	0.15	**1.79**	0.73
O-2–4	2.3	11.01	1.20	1.31	24.70	3.33	9.05	44.80	<0.01	0.02	0.46	0.15	**1.80**	0.72
O-2–5	2.1	11.00	1.19	1.30	24.83	3.36	9.09	44.65	<0.01	0.02	0.46	0.15	**1.79**	0.73
R-1–1	3.8	13.12	0.94	1.98	24.34	2.98	2.06	49.17	0.07	0.08	0.89	0.20	**2.15**	0.32
R-1–2	3.6	13.23	0.94	1.97	23.75	3.01	2.07	49.56	0.08	0.08	0.90	0.20	**2.16**	0.31
R-1–3	4.3	13.11	0.94	1.98	23.83	3.00	2.12	49.59	0.08	0.08	0.90	0.21	**2.14**	0.31
R-1–4	3.8	13.13	0.93	1.99	24.12	2.99	2.08	49.30	0.07	0.08	0.89	0.20	**2.15**	0.32
R-1–5	4.0	13.36	0.95	2.03	23.64	3.00	2.11	49.46	0.08	0.09	0.89	0.20	**2.16**	0.32

[§]Vanadium values are reported here as V not V_2O_5 for ease of comparison with the following deportment analysis—see Table A 5 for calculation of analytical totals

methods used are robust enough to reliably determine such differences, which are essential for a deportment analysis.

3.2 Phase Composition

The phase composition of the three slag samples was quantified by two complementary analytical methods, namely, XRD and AM. Because of the complexity of the phase composition, it was deemed appropriate to cross-validate between the two methods. The phase contents determined by XRD are summarized in Table 5. Since the amount of amorphous glass phases can be considered to be negligible in BOS [30–32, 40], the XRD data report the sum of all crystalline phases. Tables 6 and A 8 report the phase composition as obtained by AM analyses. Comparison reveals the generally good correspondence between the results obtained by XRD and AM, but also qualitative differences.

Qualitative differences are mainly due to the presence of different members of solid solution series. Marked by different chemical compositions, such members are easily distinguished by AM, while the presence of complex solid solutions will lead only to peak broadening in diffractograms that is best addressed by aggregating solid solution series members. XRD on the other hand is able to distinguish between polymorphs (e.g., Ca carbonates) and easily recognizes different Fe oxides. To ease comparison and further data treatment, solid phase abundance data were suitably grouped.

AM measurements revealed the presence of more than 10 different phase groups including iron and iron oxides, a magnesiowuestite-wuestite solid solution series, brownmillerite, larnite, Ca carbonates, and lime. In addition, silicates (e.g.,

feldspars) and quartz were identified. It must be noted that a significant number of the identified phases display a large heterogeneity in their chemical composition. Therefore, phases were grouped to allow a better overview of the types of phases present. Figure 4 illustrates the intergrowth relationships of the individual phases in the slag particles.

Some notable differences in phase composition can be observed between the R sample on the one hand and the two O samples on the other hand. "Ca carbonates" (which subsume calcite, dolomite, and ankerite), quartz, Mg-wuestite, larnite, metallic iron, brownmillerite, åkermanite, portlandite, and CaO (lime) are present in all three samples, while the presence of ferrite is limited to the two O samples. The R sample, besides the absence of ferrite, is characterized by the presence of gehlenite, coulsonite, and magnetite. Gehlenite represents the Mg- and Na-free end member of the melilite solid solution series [41, 42] to which also åkermanite belongs. This difference can be attributed to the different Ca/Mg ratios in the R and O slag samples. Magnetite belongs to the spinel group with possible solid solution series with, e.g., chromite and coulsonite [43–45]. Broad XRD peaks of magnetite indicate the presence of at least one of these solid solutions (e.g., coulsonite). Its presence was, however, not verified by AM.

3.3 Phase Chemistry

The chemical composition of different phases identified by AM and XRD was studied by EPMA using two polished samples for each of the three BOS samples. This was done to constrain the

Table 5 Phase composition of slag samples determined by quantitative XRD (Rietveld method) including 3 σ values. The results are reported individually for every one of the three samples created from each of the sub-samples supplied for this study

Sample	Ca carbonates* wt.%	Quartz wt.%	Mg-wuestite wt.%	Larnite wt.%	Iron wt.%	Brownmillerite wt.%	Akermanite wt.%	Portlandite wt.%	Ferrite wt.%	CaO wt.%	Gehlenite wt.%	Magnetite*** wt.%	Sum**
O-1-1	16.8 ±0.9	0.8 ±0.2	25.6 ±0.5	20.8 ±0.5	0.8 ±0.2	20.8 ±0.5	4.7 ±0.4	2.7 ±0.2	5.0 ±0.4	2.1 ±0.2			100.0
O-1-2	16.8 ±0.9	0.9 ±0.2	25.8 ±0.5	21.1 ±0.5	0.6 ±0.1	20.7 ±0.4	4.8 ±0.4	2.5 ±0.2	4.6 ±0.3	2.2 ±0.2			100.0
O-1-3	18.7 ±0.87	1.5 ±0.2	25.7 ±0.5	20.1 ±0.5	0.7 ±0.1	20.5 ±0.4	4.2 ±0.6	1.9 ±0.1	4.8 ±0.5	1.9 ±0.1			100.0
O-1-4	17.7 ±0.9	0.8 ±0.2	25.5 ±0.5	20.5 ±0.5	0.8 ±0.1	20.4 ±0.4	4.7 ±0.4	2.5 ±0.2	5.0 ±0.5	2.2 ±0.1			100.0
O-1-5	20.2 ±0.9	0.9 ±0.2	25.3 ±0.5	19.7 ±0.5	0.7 ±0.1	19.7 ±0.5	4.7 ±0.4	2.1 ±0.1	4.9 ±0.5	1.9 ±0.1			100.0
O-2-1	14.2 ±0.9	0.9 ±0.2	23.7 ±0.5	24.3 ±0.5	0.7 ±0.1	21.2 ±0.5	2.1 ±0.3	2.0 ±0.2	7.1 ±0.4	3.8 ±0.2			100.0
O-2-2	14.2 ±0.9	1.0 ±0.2	22.2 ±0.5	25.5 ±0.5	0.6 ±0.1	20.7 ±0.5	2.7 ±0.4	2.8 ±0.2	6.8 ±0.4	3.6 ±0.1			100.0
O-2-3	16.9 ±0.8	1.4 ±0.2	21.7 ±0.5	24.3 ±0.5	0.6 ±0.1	20.5 ±0.5	2.6 ±0.4	2.2 ±0.2	6.6 ±0.4	3.2 ±0.1			100.0
O-2-4	16.0 ±0.8	1.0 ±0.2	22.3 ±0.5	24.4 ±0.5	0.6 ±0.1	20.8 ±0.2	2.5 ±0.3	2.1 ±0.2	6.7 ±0.3	3.6 ±0.1			100.0
O-2-5	15.5 ±0.9	1.5 ±0.2	22.2 ±0.5	24.8 ±0.5	0.5 ±0.1	20.7 ±0.5	2.3 ±1.0	2.2 ±0.2	6.7 ±0.4	3.6 ±0.1			100.0
R-1-1	18.0 ±1.0	1.6 ±0.2	9.1 ±0.4	26.6 ±0.6	0.9 ±0.1	28.0 ±0.5	3.5 ±0.5	2.4 ±0.2		2.9 ±0.2	1.3 ±0.4	5.6 ±0.5	100.0
R-1-2	16.1 ±1.0	1.5 ±0.2	8.5 ±0.4	27.2 ±0.7	0.8 ±0.1	28.4 ±0.5	3.8 ±0.5	3.6 ±0.2		3.4 ±0.2	1.3 ±0.3	5.6 ±0.5	100.0
R-1-3	17.5 ±1.0	1.5 ±0.2	8.6 ±0.4	26.0 ±0.7	0.9 ±0.1	28.0 ±0.5	3.9 ±0.6	3.7 ±0.2		3.2 ±0.2	1.3 ±0.4	5.5 ±0.5	100.0
R-1-4	17.3 ±1.0	1.3 ±0.2	9.0 ±0.4	26.7 ±0.6	0.8 ±0.1	28.7 ±0.5	3.6 ±0.5	2.9 ±0.2		3.1 ±0.2	1.2 ±0.3	5.3 ±0.4	100.0
R-1-5	19.2 ±1.0	1.4 ±0.2	9.4 ±0.4	23.7 ±0.6	1.2 ±0.2	28.0 ±0.5	3.5 ±0.6	3.0 ±0.2		2.8 ±0.2	1.4 ±0.4	6.5 ±0.5	100.0

*"Ca carbonates" subsume calcite, dolomite, and aragonite determined by XRD. The ± data at each measured value correspond to the values for 3σ

**Normalized to 100% based on the expectation that amorphous phases are absent

***Magnetite summarizes different phases (solid solutions) of the magnetite-chromite-coulsonite solid solution series (?), which cannot be separated by XRD

Table 6 Phase composition of slag samples determined by AM[§]. The results are reported individually for every one of the sub-samples created from each of the three samples supplied for this study

Mineral	Brownmillerite wt.-%	Ca carbonate wt.-%	Lime wt.-%	Portlandite wt.-%	(Mg)-wuestite wt.-%	Larnite wt.-%	Feldspar wt.-%	Iron oxide wt.-%	Quartz wt.-%	Others wt.-%	Total wt.-%
O-1-TP1	14.2	29.4	1.6	14.4	20.9	15.0	0.2	0.4	0.0	4.1	100.0
O-1-TP2	14.6	30.4	1.7	10.6	20.9	18.5	0.2	0.2	0.1	2.9	100.0
O-1-TP3	14.5	31.1	2.0	10.7	21.3	17.5	0.0	0.1	0.0	2.8	100.0
O-1-TP5	13.9	28.3	1.3	18.9	19.9	13.1	0.0	0.2	0.0	4.4	100.0
O-1-TP6	13.3	32.8	1.4	12.5	19.0	17.3	0.0	0.2	0.0	3.5	100.0
O-2-TP1	15.0	34.3	1.0	12.2	20.3	16.1	0.0	0.1	0.0	1.1	100.0
O-2-TP2	14.8	33.6	2.2	9.7	19.6	18.8	0.1	0.2	0.1	1.0	100.0
O-2-TP4	18.7	28.1	0.8	13.1	22.2	15.7	0.0	0.1	0.0	1.3	100.0
O-2-TP5	15.6	33.1	0.9	12.2	20.6	16.4	0.1	0.1	0.0	1.1	100.0
O-2-TP6	14.8	34.6	1.9	10.6	19.4	17.4	0.1	0.3	0.1	0.9	100.0
R-1-TP1	19.9	29.1	1.7	10.2	10.4	25.0	1.0	0.7	0.8	1.3	100.0
R-1-TP2	19.2	29.0	1.2	12.2	11.0	24.1	0.2	1.2	0.3	1.8	100.0
R-1-TP3	19.3	29.7	2.4	7.9	11.2	27.4	0.5	0.3	0.4	0.7	100.0
R-1-TP4	20.8	27.4	1.3	12.7	10.7	23.8	0.5	0.4	0.3	2.1	100.0
R-1-TP6	16.3	34.7	2.6	9.2	10.1	24.6	0.7	0.4	0.3	1.2	100.0

[§]Note that AM results are typically not reported with analytical uncertainties, which can be calculated using the approach of [18]

concentration range of vanadium in major and minor phases. The phases and number of points per phase to be analyzed by EPMA were defined based on the results of XRD and AM analyses—based on the modal abundances of the different phases and expected vanadium contents (see Table A9). A total of 13 phase (groups) were thus selected for analyses (Table 6).

All analytical results were checked for conclusiveness, since the analyzed grains were often very fine-grained or very closely intergrown. Mixed analyses were thus very common. Only results that could be unequivocally assigned to a specific phase are reported in Table A10. A summary of these results with the mean values and 95% confidence intervals of every sample is provided in Tables A11–A13.

The results illustrate that larnite, brownmillerite, and portlandite are the main carriers of vanadium in the investigated BOS samples. These three minerals, together with Ca carbonates, also dominate the mineralogy of the BOS (Tables 5 and 6). They do not only form the matrix of the slag but are also almost always rather heterogeneous in their chemical composition. This manifests itself on the one hand in the formation of a classical zonation (see Fig. 4F, H) and on the other hand in complex irregular patterns reminiscent of displacement processes (see Fig. 4B, D).

4 Hydration of BOS

Strong hydration of the BOS samples was evident at all stages of the study. This was most evident for the R sample that readily agglomerated after each comminution step. This led to "clogging" of the sieve trays and other mechanical parts. The results of a hydration experiment carried out on all three BOS samples (summarized in Table A6) illustrate the extent of the hydration process as the water content was found to increase three to four times the value recorded for the initial samples delivered for this study. Under the experimental conditions we have chosen, we can assume that no significant amounts of CO_2 have been incorporated during the hydration experiments [40, 46]. The effects of hydration must, of course, be taken into careful account in all attempts of slag valorization. Hydration has, on the other hand, no effect on the deportment of vanadium that is the focus of this study.

5 Discussion

The goal of the present study is to quantify the deportment of vanadium in V-rich BOS. This requires the integration of bulk chemistry, phase abundance, and phase chemistry (e.g., vanadium content in the different phases) data [18]. The bulk chemistry data obtained for five sub-samples of each studied BOS yielded uniform results, indicating that sampling and sub-sampling procedures were successful to retain a representative composition. The phase composition and phase chemistry data, in contrast, are marked by very significant variability for all three BOS samples. The latter confirms the well-known microscale compositional complexity of slags as technological products [40, 47, 48].
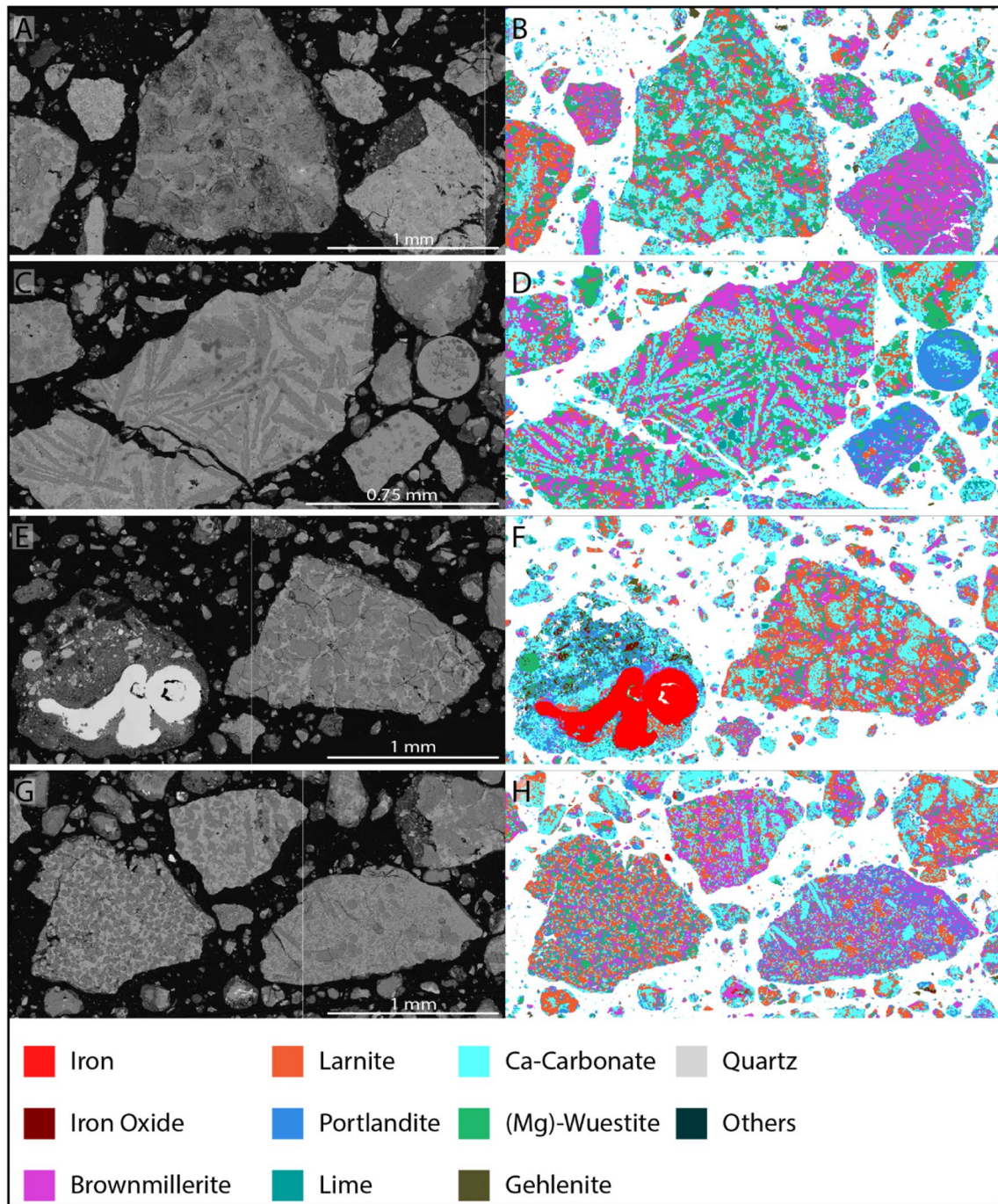
Fig. 4 Typical BSE (**A**, **C**, **E**, **G**) and classified AM (**B**, **D**, **F**, **H**) images (same image section and magnification, respectively) showing the complexity of intergrowths and associations of different phases in the BOS sample. **A**, **B** Sample O-1-TP1 with large angular slag particles composed of < brownmillerite or larnite matrix containing multiple inclusions of other slag phases. **C**, **D** Sample O-1-TP2. One very large (broken) angular particle with brownmillerite matrix containing an abundance of dendrite-like zoned Ca carbonate and smaller equigranular (Mg)-wuestite crystals. Note also smaller spherical particles with a portlandite matrix. **E**, **F** Sample R-1-TP6, rounded particle with a core of iron metal surrounded by a matrix of Ca carbonate with many portlandite and (Mg)-wuestite inclusions (partly also spherical). The second large particle in this figure consists of Ca carbonate crystals with larnite-dominated rims and brownmillerite and (Mg)-wuestite as interstitial phases. **G**, **H** Sample R-1-TP1. This image shows a variety of particles with complex larnite–Ca carbonate–portlandite–brownmillerite intergrowths. In some cases, larger Ca carbonate crystals occur

5.1 Deportment Model

To make robust estimates of the vanadium deportment for the three samples and estimate the associated uncertainties, results from AM and EPMA measurements were integrated using Monte-Carlo simulations following the method of [18]. Deportments quantitatively describe the allocation of an element to different phases in a sample and are a key factor in the recovery of minor and trace metals from different raw materials. For the present study, vanadium deportment was defined by the set of percentages:

$$\left\{ \frac{c_i \cdot x_i}{C_V} \cdot 100\% \right\}_{i=1,\ldots,N} \tag{1}$$

where c_i is the vanadium concentration in phase i, x_i is the modal abundance of phase i (in wt.%), and C_V is the bulk vanadium concentration in the sample [18].

Table 7 provides an overview of the V-bearing phases considered in the deportment calculation including their densities. A relative uncertainty of 5% was assumed for these density values, reflecting uncertainties related to porosity and density variations with phase composition. It is important to note that no actual vanadium phases such as the ternary compound $Ca_7V_2Si_2O_{16}$ [49], vanadium garnets like goldmanite [50] or momoiite [51], or pure coulsonite [45] were identified, despite the studied samples containing bulk concentrations of 1.7–2.2 wt.% of V (Table 4). This suggests that the vanadium occurs as a minor component in solid solutions—in good agreement with [52]. Table A 14 lists the modal abundances of these phases in the three studied BOS samples, including the corresponding 95% confidence intervals (CI) as estimated from the AM data. These numbers correspond to the set of x_i in Eq. (1). Table A 15 then gives an overview of the vanadium

concentrations in each phase, corresponding to the set of c_i in Eq. (1). The contribution to the deportment (Table A 15) versus the modal mineralogy is illustrated in Fig. 5. Finally, the absolute contributions of each phase to the bulk vanadium contents of the samples are shown in Table A 16.

The most important vanadium host phases in all three samples appear to be the various members of the larnite group (representing a solid solution in the system $CaO-V_2O_5-SiO_2$ described in [52]) and members of the brownmillerite group as well as portlandite. In O-1 and O-2, calcium carbonate phases are also relevant hosts. Importantly, vanadium appears to be rather evenly distributed across 3–6 distinct phases/phase groups, each containing no more than one-third of the total vanadium content in the sample.

5.2 Validation

To test the deportment results for consistency with the measured bulk V contents determined by XRF (Table 4), the results of the deportment model were used to back-calculate V contents for the three samples. The results are shown in the last line of Table 8. It is evident that back-calculated V concentrations are consistently and significantly lower than chemically determined concentrations. Nevertheless, it is remarkable that mean values rather consistently reach between 58 and 60% of the chemically measured V contents as reported in Table 4. There are several possible reasons that may contribute to this systematic discrepancy. Possible reasons include the following:

a) The study may have failed to identify a phase with high vanadium concentrations in all three samples. Yet, this explanation appears highly unlikely as such a phase

Table 7 Phases used for deportment analysis including densities used for deportment modeling

	Ideal formula	Major impurities (> 1 wt.%)	Density [g/cm³]	Standard error [g/cm³]
Brownmillerite I (high Al)	$Ca_2(Al,Fe)_2O_5$	V, Ti, Cr, Mg, Si	3.7	0.2
Brownmillerite II (medium Al)	$Ca_2(Al,Fe)_2O_5$	Ti, V, Cr, Mn, Mg, Si	3.7	0.2
Brownmillerite III (low Al)	$Ca_2(Al,Fe)_2O_5$	Mn, V, Cr, Ti, Si	3.7	0.2
Calcium carbonate	$CaCO_3$	Mg, Fe, Mn, Si in some samples	2.9	0.2
Lime	CaO	Fe, Mn, Mg	3.3	0.2
Portlandite	$Ca(OH)_2$	Fe, Si, Mn, Mg, V	2.2	0.2
Magnesiowuestite I (high Mg)	$(Fe,Mg)O$	Mn, Ca, Cr	4	0.2
Magnesiowuestite II (low Mg)	$(Fe,Mg)O$	Mn, Ca, Cr	4.5	0.2
Wuestite I (high Mg)	FeO	Mg, Mn, Ca, Cr	4.9	0.3
Wuestite II (low Mg)	FeO	Mg, Mn, Ca, Cr	5.3	0.2
Larnite	Ca_2SiO_4	P, V, Fe	3.3	0.2
Larnite (V)	Ca_2SiO_4	V, P	3.3	0.2
Native iron	Fe	Mn	7.8	0.4
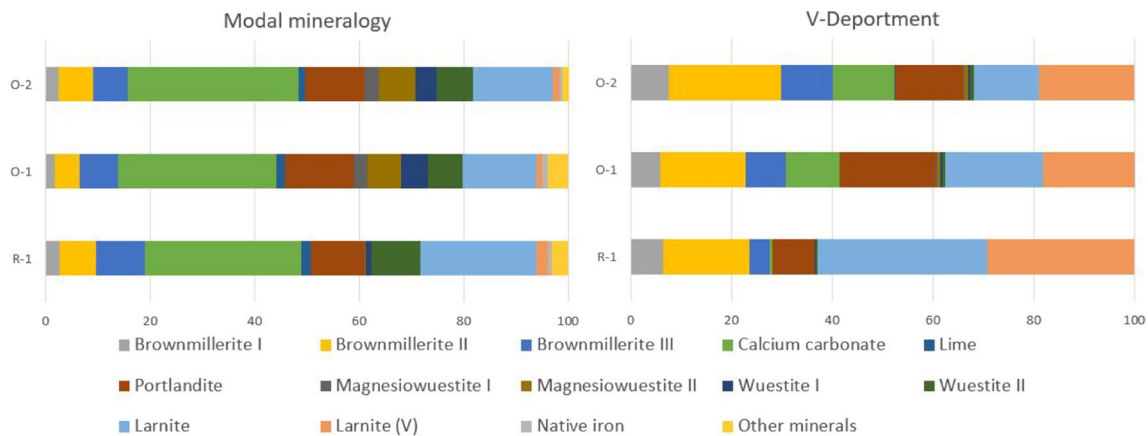
Fig. 5 Modal mineralogy as determined by AM versus the V contribution to the deportment of the respective minerals

Table 8 Phase contributions to overall V content (wt.%) with 95% confidence intervals and the resulting calculated vanadium content for the three BOS samples (last line in bold)

	R-1	O-1	O-2
Brownmillerite I	0.08 (0.06–0.09)	0.06 (0.05–0.07)	0.08 (0.07–0.09)
Brownmillerite II	0.20 (0.18–0.23)	0.16 (0.14–0.18)	0.23 (0.20–0.26)
Brownmillerite III	0.05 (0.01–0.23)	0.08 (0.06–0.10)	0.10 (0.07–0.14)
Calcium carbonate	0.00 (0.00–0.01)	0.10 (0.06–0.16)	0.12 (0.07–0.23)
Lime	0.00 (0.00–0.00)	0.00 (0.00–0.00)	0.00 (0.00–0.00)
Portlandite	0.10 (0.07–0.13)	0.18 (0.13–0.25)	0.14 (0.10–0.19)
Magnesiowuestite I	0.00 (0.00–0.00)	0.00 (0.00–0.01)	0.00 (0.00–0.00)
Magnesiowuestite II	0.0 (0.0–0.0)	0.01 (0.00–0.01)	0.01 (0.00–0.01)
Wuestite I	0.00 (0.00–0.00)	0.00 (0.00–0.01)	0.00 (0.00–0.00)
Wuestite II	0.00 (0.00–0.01)	0.00 (0.00–0.01)	0.01 (0.01–0.01)
Larnite	0.39 (0.32–0.49)	0.18 (0.13–0.25)	0.13 (0.10–0.17)
Larnite (V)	0.34 (0.29–0.40)	0.17 (0.14–0.20)	0.19 (0.16–0.22)
Native iron	0.0 (0.0–0.0)	0.00 (0.00–0.00)	0.0 (0.0–0.0)
Other minerals	0.0	0.0	0.0
Total	**1.18 (1.07–1.38)**	**0.96 (0.86–1.06)**	**1.02 (0.92–1.14)**

would need to occur in significant—and similar—amounts (>> 1 wt.%) in all three studied slag samples.

b) The modeled vanadium contents in the analyzed phases are incorrect, especially the phases that were calculated with medium vanadium concentrations (see Table A 14). The influence of such individual errors can, in the worst case, add up and not cancel each other out and have a significant impact on the back-calculated bulk composition. Although we cannot entirely exclude this source of error, we regard its impact as rather small, because the deviation of the back-calculated vanadium concentrations from the chemically determined contents are just too consistent to be related to spurious deviations.

c) A clearly noticeable source of discrepancy is the sample preparation for XRF analysis. On the one hand, ignition causes a significant loss of mass due to the release of components like H_2O and CO_2 from various phases such as portlandite and Ca carbonates, which is counteracted by the oxidation of other components like iron. This leads to an inconsistent change in the analyzed masses and consequently reduces the comparability between results from XRF and AM and XRD likewise, but it is unlikely to be responsible for the consistent deviation observed here.

d) The use of idealized densities for the phases/phase groups used the for deportment modeling [53] may be a significant source of error. Many phases present in the BOS samples are members of complex solid solution series. In addition, phases involved in the hydration processes exhibit distinct porosities. These effects may result in large and rather consistent deviations from density values reported for compositional end members in literature. The effect of this error is easily illustrated. For instance, a relative increase of 30% in the density of the larnite phases—the most important hosts of vanadium in our deportment model, compared to the other phases present in the sample would result in an increase of 5–10% in the back-calculated vanadium concentration, respectively.

Although several possible sources of error can thus be identified, we deem poorly constrained densities of

V-bearing phases as the greatest single source of error in our deportment model, resulting in significant and consistent underestimation of bulk vanadium contents, respectively.

6 Conclusions

This study introduces a comprehensive workflow for quantitative characterization and quantitative deportment of metal distribution on slags. Preservation of representativeness of sampling and sub-sampling processes is found to be equally important as the consistent/coherent identification of slag phase—in a phase system marked by an abundance of compositional variability and solid solution series. Results clearly illustrate that the combination of complementary methods like XRF and EPMA with AM is needed to provide a sound understanding of the phase composition and metal deportment of slags.

The results obtained also allow for a first, cautious geometallurgical evaluation of technological opportunities for V recovery from BOS. In the analysis of the three studied vanadium-rich BOS, no phases were identified that contain vanadium in stoichiometric amount—and not single phase (group) dominates the deportment of vanadium. The bulk of vanadium is bound in Ca-rich solid solution series—(almost) none occurs in spinel or wuestite phases. The vanadium-bearing minerals constitute a very large mass fraction of the BOS. Any effort to extract vanadium from these slags will thus necessitate the chemical processing of the bulk material—with no opportunity to significantly enrich vanadium-bearing hosts by physical beneficiation processes.

In a highly generalized view, these results show that, even for the utilization of secondary raw material sources such as slags, an evaluation by simple bulk chemical investigations will not provide sufficient results. In order to decide which principal routes of physical treatment and/or chemical processing are suitable for beneficiation and metal extraction, comprehensive (i.e., geometallurgical) characterization of the samples is mandatory.

Data Availability All data used in this study are listed in the article or in the electronic supplementary material.

Declarations

Conflict of interest The authors declare no competing interests.

References

1. worldsteel.org, Total production of crude steel, (23.04.2023). https://worldsteel.org/steel-topics/statistics/annual-production-steel-data/?ind=P1_crude_steel_total_pub/CHN/IND. Accessed 15 Sept 2023

2. Wang Z, Sohn I (2019) A review on reclamation and reutilization of ironmaking and steelmaking slags. J Sustain Metall 5(1). https://doi.org/10.1007/s40831-018-0201-5

3. Anonymous (2012) Position paper status of ferrous slag complying with the waste framework directive (articles 5/6) and the REACH regulation 32. https://www.euroslag.com/wp-content/uploads/2019/01/Position_Paper_April_2012.pdf. Accessed 15 Sept 2023

4. Jochims K, Bialucha R (2019) Toxicological investigations of ferrous slag in the context of the REACH registration (1–2019). https://www.euroslag.com/wp-content/uploads/2019/09/Report-1-2019-REACH-englisch.pdf. Accessed 15 Sept 2023

5. Guo J, Bao Y, Wang M (2018) Steel slag in China: treatment, recycling, and management. Waste Manag 78. https://doi.org/10.1016/j.wasman.2018.04.045

6. Horckmans L, Möckel R, Nielsen P, Kukurugya F, Vanhoof C, Morillon A, Algermissen D (2019) Multi-analytical characterization of slags to determine the chromium concentration for a possible re-extraction. Minerals 9(10). https://doi.org/10.3390/min9100646

7. Seetharaman S, Wang L, Wang H (2022) Slags containing transition metal (chromium and vanadium) oxides—conversion from ticking bombs to valuable resources: Collaborative studies between KTH and USTB. Int J Miner Metall Mater 29(4). https://doi.org/10.1007/s12613-022-2424-5

8. Gustafsson JP, Johnsson L (2004) VANADIN I SVENSK MILJÖ, TRITA-LWR Report 3009

9. Kotaś J, Stasicka Z (2000) Chromium occurrence in the environment and methods of its speciation. Environ Pollut 107(3). https://doi.org/10.1016/S0269-7491(99)00168-2

10. Wnuk E (2023) Mobility, bioavailability, and toxicity of vanadium regulated by physicochemical and biological properties of the soil. J Soil Sci Plant Nutr 23(1). https://doi.org/10.1007/s42729-023-01130-9

11. Peng H, Guo J, Li B, Huang H (2022) Vanadium properties, toxicity, mineral sources and extraction methods: a review. Environ Chem Lett 20(2). https://doi.org/10.1007/s10311-021-01380-y

12. European Commission D.-G. f. I. M., Industry, entrepreneurship and SMEs, Proposal for a regulation of the European Parliament and of the council establishing a framework for ensuring a secure and sustainable supply of critical raw materials and amending regulations (EU) 168/2013, (EU) 018/858, 2018/1724 and (EU) 2019/1020, *European Commission, Directorate-General for Internal Market, Industry, Entrepreneurship and SMEs*, 16.03.2023, COM/2023/160 final: 94

13. European Commission (2023) Directorate General for Internal Market I. E. S., Study on the critical raw materials for the EU 2023: final report, Edited, Publications Office, Brussels, p 160 https://doi.org/10.2873/725585

14. Gilligan R, Nikoloski AN (2020) The extraction of vanadium from titanomagnetites and other sources. Miner Eng 146. https://doi.org/10.1016/j.mineng.2019.106106

15. Lee J-C, Kurniawan, Kim E-Y, Chung KW, Kim R, Jeon H-S (2021) A review on the metallurgical recycling of vanadium from slags: towards a sustainable vanadium production. J Mater Res Technol 12. https://doi.org/10.1016/j.jmrt.2021.02.065

16. Pikna L, Hezelova M, Morillon A, Algermissen D, Milkovic O, Findorak R, Cesnek M, Briancin J (2020) Recovery of chromium from slags leachates by electrocoagulation and solid product characterization. Metals 10(12). https://doi.org/10.3390/met10121593

17. Yu L, Dong YC, Ye GZ, Sichen D (2007) Concentrating of vanadium oxide in vanadium rich phase(s) by addition of SiO_2 in converter slag. Ironmak Steelmak 34(2). https://doi.org/10.1179/174328107X155286

18. Frenzel M, Bachmann K, Carvalho JRS, Relvas JMRS, Pacheco N, Gutzmer J (2019) The geometallurgical assessment of by-products—geochemical proxies for the complex mineralogical deportment of indium at Neves-Corvo, Portugal. Miner Deposita 54(7). https://doi.org/10.1007/s00126-018-0849-6

19. Gregory MJ, Lang JR, Gilbert S, Hoal K O (2013) Geometallurgy of the pebble porphyry copper-gold-molybdenum deposit, Alaska: implications for gold distribution and paragenesis. Econ Geol 108(3). https://doi.org/10.2113/econgeo.108.3.463

20. Chryssoulis SL, Cabri LJ (1990) The significance of gold mineralogical balances in mineral processing. Trans Inst Min Metall, Section A: Min Technol 99

21. Osbahr I, Oberthür T, Klemd R, Josties A (2014) Platinum-group element distribution in base-metal sulfides of the UG2 chromitite, Bushveld Complex, South Africa—a reconnaissance study. Miner Deposita 49(6). https://doi.org/10.1007/s00126-014-0538-z

22. Allibert M (1995) Slag Atlas. Verlag Stahleisen, Düsseldorf

23. Alex TC, Mucsi G, Venugopalan T, Kumar S (2021) BOF steel slag: critical assessment and integrated approach for utilization. J Sustain Metall 7(4). https://doi.org/10.1007/s40831-021-00435-2

24. Min DJ, Tsukihashi F (2017) Recent advances in understanding physical properties of metallurgical slags. Metals Mater Int 23(1). https://doi.org/10.1007/s12540-017-6750-5

25. Chiang P-C, Pan S-Y, Chiang P-C, Pan S-Y (2017) Iron and steel slags. Carbon Dioxide Miner Util. https://doi.org/10.1007/978-981-10-3268-4_11

26. Piatak NM, Ettler V, Hoppe D (2021) Chapter 3 Geochemistry and mineralogy of slags, Edited. Royal Soc Chem Metall Slags: Environ Geochem Resource Potential:59–124. https://doi.org/10.1039/9781839164576-00059

27. Hryha E, Rutqvist E, Nyborg L (2012) Stoichiometric vanadium oxides studied by XPS. Surf Interface Anal 44(8). https://doi.org/10.1002/sia.3844

28. Chaurand P, Rose J, Briois V, Salome M, Proux O, Nassif V, Olivi L, Susini J, Hazemann J-L, Bottero J-Y (2007) New methodological approach for the vanadium K-edge X-ray absorption near-edge structure interpretation: application to the speciation of vanadium in oxide phases from steel slag. J Phys Chem B 111(19). https://doi.org/10.1021/jp063186i

29. Hryha E, Rutqvist E, Björkvall J, Nyborg L (2014) Development of methodology for surface characterization of vanadium containing slag, Surf Interface Anal 46(10–11). https://doi.org/10.1002/sia.5363

30. Belhadj E., Diliberto C. and Lecomte A., Characterization and activation of basic oxygen furnace slag, Cem Concr Compos 34(1). https://doi.org/10.1016/j.cemconcomp.2011.08.012

31. Bodor M, Santos RM, Cristea G, Salman M, Cizer Ö, Iacobescu RI, Chiang YW, van Balen K, Vlad M, van Gerven T (2016) Laboratory investigation of carbonated BOF slag used as partial replacement of natural aggregate in cement mortars. Cem Concr Compos 65. https://doi.org/10.1016/j.cemconcomp.2015.10.002

32. Santos RM, Ling D, Sarvaramini A, Guo M, Elsen J, Larachi F, Beaudoin G, Blanpain B, Van Gerven T (2012) Stabilization of basic oxygen furnace slag by hot-stage carbonation treatment. Chem Eng J 203. https://doi.org/10.1016/j.cej.2012.06.155

33. Bish DL, Reynolds RC (1989) 4. Sample preparation for X-ray diffraction, Edited by L. B. David and E. P. Jeffrey, De Gruyter, Modern Powder Diffraction, Berlin, Boston, 1989: 73–100. https://doi.org/10.1515/9781501509018-007

34. Doebelin N, Kleeberg R (2015) Profex: a graphical user interface for the Rietveld refinement program BGMN. J Appl Crystallogr 48. https://doi.org/10.1107/s1600576715014685

35. Heinig T, Bachmann K, Tolosana-Delgado R, Van Den Boogaart G, Gutzmer J (2015) Monitoring gravitational and particle shape settling effects on MLA sampling preparation. Proceedings of the IAMG, pp 200–206

36. Gu Y (2003) Automated scanning electron microscope based mineral liberation analysis An introduction to JKMRC/FEI mineral liberation analyser. J Miner Mater Charact Eng 2(1). https://doi.org/10.4236/jmmce.2003.21003

37. Fandrich R, Gu Y, Burrows D, Moeller K (2007) Modern SEM-based mineral liberation analysis. Int J Miner Process 84(1–4). https://doi.org/10.1016/j.minpro.2006.07.018

38. Bachmann K, Frenzel M, Krause J, Gutzmer J (2017) Advanced identification and quantification of In-bearing minerals by scanning electron microscope-based image analysis. Microsc Microanal 23(3). https://doi.org/10.1017/S1431927617000460

39. Osbahr I, Krause J, Bachmann K, Gutzmer J (2015) Efficient and accurate identification of platinum-group minerals by a combination of mineral liberation and electron probe microanalysis with a new approach to the offline overlap correction of platinum-group element concentrations. Microsc Microanal 21(5). https://doi.org/10.1017/s1431927615000719

40. Vollprecht D, Wohlmuth D (2022) Mineral carbonation of basic oxygen furnace slags. Recycling **7**(6). https://doi.org/10.3390/recycling7060084

41. Stavrakeva D, Georgieva I (1995) New data on the composition of melilite during solid phase and solid-liquid phase synthesis. Comptes Rendus-Academie Bulgare des Sciences 48(9–10)

42. Deer WA, Howie RA, Zussman J (2013) An introduction to the rock-forming minerals, Edited, Mineralogical Society of Great Britain and Ireland. https://doi.org/10.1180/dhz

43. Reznitsky LZ, Sklyarov EV, Suvorova LF, NS K (2005) The chromite-coulsonite-magnetite solid solution: The first find of a rare variety of spinel in terrestrial rocks. Doklady Earth Sci 404(7)

44. Wang YG, Ye HQ, Ximen LL, Kuo KH (1989) A HREM study of the intergrowth of magnetite and coulsonite. Acta Crystallogr Section A 45(4). https://doi.org/10.1107/S0108767388012231

45. Radtke AS (1962) Coulsonite, FeV_2O_4, a spinel-type mineral from Lovelock, Nevada. Am Miner 47(11–12)

46. Huijgen WJJ, Witkamp G-J, Comans RNJ (2005) Mineral CO_2 sequestration by steel slag carbonation. Environ Sci Technol 39(24). https://doi.org/10.1021/es050795f

47. Waligora J, Bulteel D, Degrugilliers P, Damidot D, Potdevin JL, Measson M (2010) Chemical and mineralogical characterizations of LD converter steel slags: a multi-analytical techniques approach. Mater Charact 61(1). https://doi.org/10.1016/j.matchar.2009.10.004

48. Schollbach K, Laan Svd (2021) Chapter 3 Microstructure analysis with quantitative phase mapping using SEM-EDS and Phase Recognition and Characterization (PARC) Software: applied to steelmaking slag. H Pöllmann, De Gruyter (ed) Industrial Waste, Berlin, Boston, pp 57–96. https://doi.org/10.1515/9783110674 941-003

49. Rain M, Berman S, McCauley R (1980) Compatibility triangles in the system $CaO-V_2O_5-SiO_2$. J Am Ceram Soc 63(3–4). https://doi.org/10.1111/j.1151-2916.1980.tb10709.x

50. Moench RH, Meyrowitz R (1964) Goldmanite, a vanadium garnet from Laguna, New Mexico. Am Min 49(5–6)

51. Tanaka H, Endo S, Minakawa T, Enami M, Nishio-Hamane D, Miura H, Hagiwara A (2010) Momoiite, $(Mn^{2+},Ca)_3(V^{3+},Al)_2Si_3O_{12}$, a new manganese vanadium garnet from Japan. J Min Petrol Sci 105(2). https://doi.org/10.2465/jmps.091015a

52. Jantzen T, Yazhenskikh E, Hack K, Baben Mt, Wu G, Müller M (2021) Addition of V_2O_5 and V_2O_3 to the $CaO–FeO–Fe_2O_3–MgO–SiO_2$ database for vanadium distribution and viscosity calculations. Calphad 74. https://doi.org/10.1016/j.calphad.2021.102284

53. Balonis M, Glasser FP (2009) The density of cement phases. Cement Concr Res 39(9). https://doi.org/10.1016/j.cemconres.2009.06.005

Publisher's Note Springer Nature remains neutral with regard to jurisdictional claims in published maps and institutional affiliations.